

Methionine Residue Acts as a Prooxidant in the $\bullet\text{OH}$ -Induced Oxidation of Enkephalins

Olivier Mozziconacci,^{†,‡,§} Jacek Mirkowski,[‡] Filippo Rusconi,^{||,†} Gabriel Kciuk,[‡] Pawel B. Wisniowski,[‡] Krzysztof Bobrowski,^{*,‡} and Chantal Houée-Levin^{*,†}

[†]Laboratory of Physical Chemistry and CNRS Bldg 350, Centre Universitaire, F-91405 Orsay, F-91405 Orsay, France

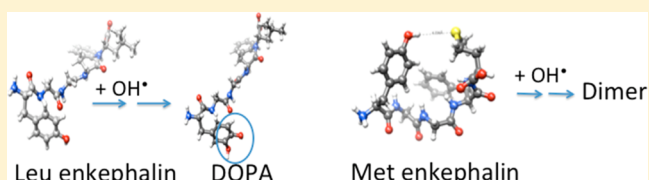
[‡]Institute of Nuclear Chemistry and Technology, Dorodna, 16, 03-195 Warsaw, Poland

[§]Department of Pharmaceutical Chemistry, University of Kansas, Lawrence, Kansas 66047, United States

^{||}Muséum National d'Histoire Naturelle, CNRS, UMR7196 - INSERM, U565 - MNHN USM0503, 57 rue Cuvier, F-75231 Paris Cedex-05, France

S Supporting Information

ABSTRACT: Enkephalins are bioactive pentapeptides (Tyr-Gly-Gly-Phe-Leu (Leu-enk) and Tyr-Gly-Gly-Phe-Met (Met-enk)) produced while an organism is under mental and/or physical stress. In the course of their biological action they are exposed to reactive oxygen and nitrogen species. We have reinvestigated the reactions of $\bullet\text{OH}$ radicals toward these peptides in order to elucidate the oxidation mechanisms and the final products. Nanosecond pulse radiolysis was used to obtain the spectra of the reaction intermediates and their kinetics. Additional insight into details of the oxidation mechanism was gained by identification of main final products by means of UV-vis spectrophotometry, HPLC coupled with fluorescence spectroscopy, and mass spectrometry. The key processes are different in both peptides. In Leu-enk, the first step is an $\bullet\text{OH}$ radical addition to the aromatic rings of Tyr and Phe residues that leads to hydroxylated residues, dihydroxyphenylalanine (DOPA) from Tyr and tyrosine isomers from Phe, respectively. In Met-enk, these processes are less important, an additional target being the sulfur atom of the methionine residue. Depending on pH either an OH-adduct (hydroxysulfuranyl radical) or a sulfur radical cation undergo intramolecular electron transfer with Tyr residue resulting in a repair of Met and oxidation of Tyr to tyrosyl radicals and a final formation of dityrosine. At low pH, the OH-adducts to Tyr residue are precursors of tyrosyl radicals and dityrosine. Thus, the final products coming from oxidation of the Tyr residue depend strongly on the neighboring residues and the pH.



INTRODUCTION

There is substantial evidence that oxidative stress is a causative factor in the pathogenesis of several major diseases including both neurodegenerative Parkinson's¹ and Alzheimer's diseases.² Protein modifications are known to play major roles in these diseases. The consequences of protein oxidation are not well-known because they depend on the possibility either to destroy the damaged ones or to repair the oxidized residues by reduction. Tyrosine is one of the main targets of reactive oxygen and nitrogen species (RONS, i.e., $\bullet\text{OH}$, $\text{O}_2^{\bullet-}$, NO^\bullet , hydrogen peroxide, peroxyxynitrite, etc.). When its oxidation leads to polymerization, toxic protein aggregates are formed.³ On the other hand, methionine, another main target of oxidative stress, is usually considered as a protective residue against RONS since one major final product, methionine sulfoxide, can be "repaired" by reduction to the initial residue by methionine sulfoxide reductases.

Enkephalins are usually produced while the organism is under mental and/or physical stress. These bioactive peptides originate from the larger protein, β -lipotropin,⁴ and are exhibiting, as a common feature, the presence of a tyrosine residue at the N-terminus, which is essential for their biological

activity.⁵ They are distributed as a mixture of two pentapeptides, Tyr-Gly-Gly-Phe-Leu (Leu-enk) and Tyr-Gly-Gly-Phe-Met (Met-enk), in the central nervous system, specific areas of the brain, and the spinal cord, as well as in nerve plexi of intestines.⁶ These pentapeptides are opiates and have the same receptors as morphine and thebaine. Their distribution and the distribution of the opioid receptors ensure a highly effective pain management system. They play the role of neurotransmitters and neurohormones in regions of the brain and spine associated with diffuse pain pathways and inhibition of pain signals.⁷ Moreover, enkephalins are involved in all kinds of stresses,⁸ in red blood cells,⁹ as well as in liver¹⁰ and brain.¹¹ They play diverse roles in biological systems such as controlling respiration, aiding human immune response,¹² producing dependence, and tolerance to stroke.¹³ One of their important roles is the control of pain by binding to nociceptive receptors.¹⁴ In the processes occurring during development of illnesses, enkephalins are subjected to oxidation by reactive

Received: July 16, 2012

Revised: September 19, 2012

Published: September 22, 2012

oxygen species (ROS), i.e., hydroxyl radicals ($\bullet\text{OH}$), superoxide radical anions ($\text{O}_2^{\bullet-}$), and molecular products like H_2O_2 .

The degradations induced by $\bullet\text{OH}$ radicals in Met-enk and in Leu-enk are relevant to the disorders in inflammatory processes. Because of the importance of these reactions in vivo, several studies were devoted to their mechanism. In vitro experiments showed that Met-enk and Leu-enk, in the presence of hydrogen peroxide, can be oxidized by horseradish peroxidase to the enkephalin dimers with a dityrosyl bond between the N-terminal tyrosine residues.¹⁵ The same product was found when Met-enk or its precursor, pre-Met-enk, were exposed to activated oxygen species produced by stimulated polymorphonuclear leucocytes.¹⁶ Enkephalins scavenge oxygen free radicals generated by the Fenton reaction. The N-terminal tyrosine residues were found to be the main target of $\bullet\text{OH}$ radicals, which convert further into DOPA derivatives.¹⁷ In the presence of an excess of thiols the oxidation of enkephalins gives rise to S-cysteinyldopa-enkephalins.¹⁸ Nitrogen radicals (peroxynitrite and peroxidase-generated reactive nitrogen species) also react with the N-terminal Tyr residue, producing nitrotyrosine and enkephalin dimers linked by dityrosine.¹⁹

We have already investigated the oxidation mechanism of Met-enk induced by a one-electron oxidant species, the azide radicals (N_3^{\bullet}) in N_2O and O_2 -saturated solutions. The N-terminal Tyr residue was found to be the main target for oxidation. Moreover, it was demonstrated that, when $\text{O}_2^{\bullet-}$ was present, it added to tyrosyl radical, giving a hydroperoxide which further cyclized by reaction with the terminal amine.²⁰ In two recent papers the mechanism of oxidation of enkephalins by peroxidase in the presence of superoxide was investigated.²¹ The authors proposed a mechanism in which the first step of oxidation was the formation of tyrosyl radicals followed by addition of superoxide that led to tyrosine hydroperoxide.^{21a} However, in Met-enk, an intramolecular two-electron process was invoked: the reaction of the tyrosine hydroperoxide with methionine leading to methionine sulfoxide and a deoxy-generated derivative of tyrosine.

In this study we reinvestigated the one-electron oxidation of both Leu-enk and Met-enk by $\bullet\text{OH}$ radicals produced by pulse and gamma radiolysis at two pH values (6.5 and 1), to unveil the mechanisms of degradation of the tyrosine residue in both peptides. Whereas at natural pH (ca. 6.5), one gets hydroxylated tyrosine (DOPA) or phenylalanine (o- or p-tyrosine) in Leu-enk, a peptide dimer linked by dityrosine was observed in Met-enk where the major target is the methionine residue. This latter observation has been rationalized by an intramolecular one-electron transfer from the tyrosine residue to the methionine radical cation. Methionine sulfoxide, which is most commonly the final product of methionine oxidation, can be repaired in vivo by methionine sulfoxide reductases, which means that oxidation of methionine is not deleterious. However, the conversion of a methionine radical cation to a tyrosyl radical leads to a nonrepairable damage. Thus, the final products coming from tyrosine oxidation and possibly useful as biomarkers of oxidative stress are numerous. They do not only depend on the oxidant and the presence of oxygen but also on the reaction pathways.

EXPERIMENTAL AND THEORETICAL METHODS

Materials. Leu-enk (Tyr-Gly-Gly-Phe-Leu) and Met-enk (Tyr-Gly-Gly-Phe-Met) pentapeptides were purchased from Bachem (Switzerland). The other chemicals were obtained as follows: perchloric acid (HClO_4) was purchased from Sigma-

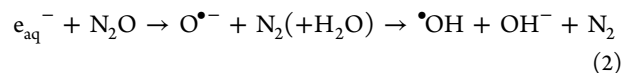
Aldrich and nitrous oxide (N_2O) 99% from the Air Liquide AlphaGaz.

All solutions were made with water triply distilled from permanganate or delivered by Elga Maxima system. The pH was adjusted by the addition of perchloric acid (HClO_4). Typical concentration of solutions (3 mL) for γ irradiation was 0.5 mM (enkephalins) at natural pH (6.5) and at pH 1.5, unless otherwise specified. Prior to irradiation, the samples were purged gently with N_2O for 20 min. Typical concentration of solutions in pulse radiolysis experiments was 0.1 mM of enkephalins at natural pH (6.5) and 1.5 unless otherwise specified. They were purged with N_2O for 30 min per 50 mL volume before experiments.

Steady-State γ -Radiolysis. γ irradiation was carried out using the ^{60}Co γ -rays source Issledovatel (USSR) in the Institute of Nuclear Chemistry and Technology (Warsaw, Poland) and the panoramic ^{60}Co γ -source IL60PL Cis-Bio International (France) in the University Paris-Sud (Orsay). The dose rates were equal to 1.05 Gy min^{-1} and 7.5 Gy min^{-1} , respectively as determined by Fricke dosimetry.²² All irradiations were performed at room temperature. The doses applied ranged between 80 and 500 Gy.

Pulse Radiolysis. Pulse radiolysis experiments were performed with the INCT LAE 10 MeV linear electron accelerator with typical pulse length of 8 ns. A detailed description of the experimental setup has been given elsewhere along with the basic details of the equipment and the data collection system.²³ Radiolytic yields are given in the Supporting Information (SI) with units as $\mu\text{mol J}^{-1}$. Absorbed doses per pulse were on the order of 5.5 Gy ($1 \text{ Gy} = 1 \text{ J kg}^{-1}$). Dosimetry was based on N_2O -saturated solutions containing 10^{-2} M KSCN , taking a radiation chemical yield of $G = 0.635 \mu\text{mol J}^{-1}$ and a molar absorption coefficient of $7580 \text{ M}^{-1} \text{ cm}^{-1}$ at 472 nm for the $(\text{SCN})_2^{\bullet-}$ radical.²⁴ Experiments were performed with a continuous flow of sample solutions at room temperature ($\sim 23^\circ\text{C}$).

Radiolysis of Water. γ or pulse irradiation of water leads to the formation of the primary reactive species shown in reaction 1. In N_2O -saturated solutions ($[\text{N}_2\text{O}]_{\text{sat}} \approx 2 \times 10^{-2} \text{ M}$), hydrated electrons, e_{aq}^- , are converted into $\bullet\text{OH}$ radicals according to reaction 2 ($k_2 = 9.1 \times 10^9 \text{ M}^{-1} \text{ s}^{-1}$).²⁵ Reaction 2 nearly doubles the amount of $\bullet\text{OH}$ radicals available for reactions with substrates.



Thus, the radiation-chemical yields (G values) of these primary species in aqueous N_2O -saturated solution at neutral pH are $G(\bullet\text{H}) = 0.06 \mu\text{mol J}^{-1}$ and $G(\bullet\text{OH}) = 0.56 \mu\text{mol J}^{-1}$ (reactions 1 and 2). At pH < 4 the diffusion-controlled reaction of e_{aq}^- with protons becomes important (reaction 3, $k_3 = 2.3 \times 10^{10} \text{ M}^{-1} \text{ s}^{-1}$)²⁶ resulting in a pH-dependent lowered yield of $\bullet\text{OH}$ radicals and a corresponding increased yield of $\bullet\text{H}$ atoms.



Therefore, in N_2O -saturated aqueous solutions at pH 1.5, taking into account the known rate constants for reactions 2 and 3, one can calculate the radiation-chemical yields for $G(\bullet\text{H}) = 0.34 \mu\text{mol J}^{-1}$ and $G(\bullet\text{OH}) = 0.28 \mu\text{mol J}^{-1}$.²²

Spectral Analysis and Resolution of Time-Resolved Optical Spectra. In any time window, following the electron pulse, the absorbance of the solution is related to the radiation-chemical yield and the molar absorption coefficients by the formula i

$$G\varepsilon(\lambda_j) = \Delta A(\lambda_j) \frac{\varepsilon_{472\text{nm}} G(\text{SCN})_2^{\bullet-}}{\Delta A_{472\text{nm}}} \quad (\text{i})$$

which are how the spectra are displayed in Figures 1 and 5.

Equation i is a convenient way to normalize the absorbance $\Delta A(\lambda_j)$ to the radiation dose, the inverse of which is proportional to $\varepsilon_{472} G((\text{SCN})_2^{\bullet-}) / \Delta A_{472}$ from thiocyanate dosimetry, where ε_{472} is the molar absorption coefficient of $(\text{SCN})_2^{\bullet-}$ at 472 nm ($7580 \text{ M}^{-1} \text{ cm}^{-1}$), $G((\text{SCN})_2^{\bullet-})$ is the radiation chemical yield of the $(\text{SCN})_2^{\bullet-}$ radicals ($0.635 \mu\text{mol J}^{-1}$), and ΔA_{472} represents the observed absorbance change at 472 nm in the thiocyanate dosimeter. The $G\varepsilon(\lambda_j)$ are in turn related to the underlying transients via Beer's Law since $\Delta A = \log(I_0/I)$ is the absorbance of the sample.

A multiregression analysis was done on the optical transient spectra monitored at various time delays following the electron pulse. They were resolved into specific components (representing individual transients) by linear regression according to equation ii

$$G \times \varepsilon(\lambda_j) = \sum_{i=1}^n G_i \times \varepsilon_i(\lambda_j) \quad (\text{ii})$$

Here $G\varepsilon(\lambda_j)$ is related to the observed absorbance change $\Delta A(\lambda_j)$ of the composite spectrum according to eq 1, G_i is the linear regression coefficient of the i th species, and $\varepsilon_i(\lambda_j)$ is the molar absorption coefficient of the i th species at the j th wavelength. Further details of this method have been described elsewhere.²⁷

The radiation chemical yields of the respective transient species in the optical spectra were calculated taking the following representative molar absorption coefficients: $\varepsilon_{290} = 4300 \text{ M}^{-1} \text{ cm}^{-1}$, $\varepsilon_{390} = 2400 \text{ M}^{-1} \text{ cm}^{-1}$, and $\varepsilon_{405} = 3000 \text{ M}^{-1} \text{ cm}^{-1}$ for tyrosyl radicals (TyrO^{\bullet}); $\varepsilon_{310} = 2900 \text{ M}^{-1} \text{ cm}^{-1}$ and $\varepsilon_{330} = 3000 \text{ M}^{-1} \text{ cm}^{-1}$ for hydroxycyclohexadienyl radicals of tyrosine $\text{TyrOH}(\bullet\text{OH})$; $\varepsilon_{340} = 5600 \text{ M}^{-1} \text{ cm}^{-1}$ for cyclohexadienyl radicals of tyrosine $\text{TyrOH}(\bullet\text{H})$; $\varepsilon_{320} = 4100 \text{ M}^{-1} \text{ cm}^{-1}$ for hydroxycyclohexadienyl radicals of phenylalanine $\text{Phe}(\bullet\text{OH})$; $\varepsilon_{320} = 5000 \text{ M}^{-1} \text{ cm}^{-1}$ for cyclohexadienyl radicals of phenylalanine $\text{Phe}(\bullet\text{H})$, $\varepsilon_{330} = 3400 \text{ M}^{-1} \text{ cm}^{-1}$ for hydroxysulfuranyl radicals of methionine $\text{Met}(\text{S}^{\bullet}\text{-OH})$, and $\varepsilon_{290} = 3000 \text{ M}^{-1} \text{ cm}^{-1}$ for α -(alkylthio)alkyl radicals of methionine $\text{MetS}(\bullet\text{CH})/\text{MetS}(\bullet\text{CH}_2)$.

Since the radiation chemical yield of $\bullet\text{H}$ atoms at $\text{pH} > 3$ is roughly 10-fold lower than that of $\bullet\text{OH}$ radicals, the contribution of cyclohexadienyl radicals during multiregression analysis procedure of the experimental spectra at natural pH was neglected. Therefore, one has to be aware that the radiation chemical yields of hydroxycyclohexadienyl radicals at natural pH might be slightly overestimated. Moreover, the error limit (within $\pm 15\%$) validates the spectra resolution and eliminates unreasonable fits. The error limit ($\pm 15\%$) allows for $\pm 5\%$ variation in the experimental data and a $\pm 10\%$ combined error in the reported molar absorption coefficients for the spectra of components under consideration.

UV-vis. The absorption spectra were recorded with the Perkin-Elmer UV-visible spectrophotometer using a 1 cm optical path length cell. Nonirradiated solutions were used as

reference solutions. An aliquot of 1 mL was taken to measure the absorption spectrum.

High Performance Liquid Chromatography (HPLC). The HPLC analyses were carried out with a Shimadzu chromatograph consisting of a pump, a 20 μL manual injector, a polymer PLRP-S 100- μm column $4.6 \times 250 \text{ mm}$, packed with 5- μm particles. The detectors were either a photodiode array detector or a spectrofluorimetric at several settings. The first setting with the excitation wavelength of 240 nm and with the emission wavelength of 285 nm was used to detect mainly a phenylalanine residue and also a tyrosine residue. The second setting with the excitation wavelength of 284 nm and with the emission wavelength of 305 nm was used to detect mainly a tyrosine residue. The third setting with the excitation wavelength of 284 nm and with the emission wavelength of 425 nm was used to detect ditirosine. The mobile phase was delivered with a flow rate of 0.9 mL min^{-1} . It consisted of two solvents, the first with 95% of water, 5% of acetonitrile and 0.01% of trifluoroacetic acid (TFA) and the second with 80% of acetonitrile, 20% of water, 0.01% trifluoroacetic acid (TFA). TFA was used to fix the pH along the separation analysis and to increase the sensitivity of the analysis (shape peaks).

All chromatography data acquisition and processing were performed using the program supplied with the Shimadzu package system.

Mass Spectrometry. All mass spectrometric experiments were performed in the positive-ion mode using a hybrid quadrupole time-of-flight mass spectrometer equipped with an electro-spray ion source (ESI MS, Q-Star Pulsar i, MDS Sciex-Applied Biosystems). Data acquisition and storage were performed using the Analyst QS software package shipped with the mass spectrometer. Sequence editing and mass calculations were typically performed using either GNU polyxmass²⁸ or massXpert.²⁹ MS experiments were performed as follows: injections in the flow of an HPLC system were performed at 30 $\mu\text{L}/\text{min}$ (carrier solvent was acetonitrile/water/formic acid, 49:50:1); the typical peptide concentration was $1.15 \times 10^{-2} \mu\text{g}/\mu\text{L}$; the ion spray needle was set to 5200 V; the declustering potential was set to 60 V; the m/z scan range was from m/z 100 to m/z 2000; the scan cycle was of 1 s. MS/MS experiments were performed at the same conditions as above, except for the following: ions were selected based on their $[\text{M}+\text{H}]^+$ m/z value, in the mass unit mode, using the Analyst QS software package and fragmentations were initiated with nitrogen as the collision gas; the declustering potential was set to 60 V; the maximum collision energy was typically of 35–40 eV.

Computations. In order to show that structures with small methionine sulfur–tyrosine (S–O) distances could be stable in water, seven different initial conformations were fully optimized using the B3LYP/6-31G* level of theory and G09 software.³⁰ The starting points were seven conformations from the Protein Data Bank (PDB 1PLW) chosen because of their different levels of folding. It should be noted that the structures deposited in the PDB were recorded not in aqueous solutions but in micelles thus the stable structures might be different from those in water. Solvation effects were accounted with the COSMO option for the polarized continuum model CPCM considering an aqueous environment. Molecular graphics images were produced using the UCSF Chimera package from the Resource for Biocomputing, Visualization, and Informatics at the University of California, San Francisco (supported by NIH P41 RR001081).³¹

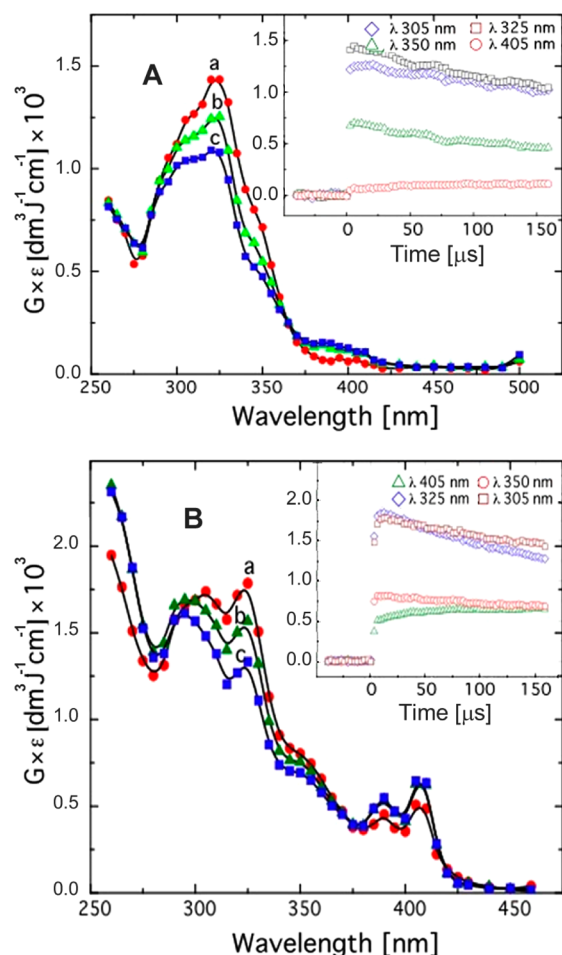


Figure 1. Transient absorption spectra recorded after the pulse irradiation in N_2O -saturated solutions containing Leu-enk (0.2 mM). A: pH 6.4 with the following time delays: 5 μs (a, red circle), 70 μs (b, green triangle), and 140 μs (c, blue square). Insets: Kinetic traces recorded at 305, 325, 350, and 405 nm. B: pH 1.0 with the following time delays: 5 μs (a, red circle), 70 μs (b, green triangle), and 140 μs (c, blue square). Insets: Kinetic traces recorded at 305, 325, 350, and 405 nm.

RESULTS

Leu-Enkephalin: Transient Species. The reaction of $\cdot\text{OH}$ radicals with Leu-enk was investigated in N_2O -saturated solutions over the concentration range of 0.1–0.6 mM, at two pH values, natural pH (no buffer, ca. 6.5) and pH 1.

Natural pH. UV-vis Transient Absorption Spectra. A transient spectrum obtained 5 μs after the electron pulse in N_2O -saturated solutions containing 0.2 mM of Leu-enk at natural pH (no buffer, pH 6.4–6.5) exhibits a broad absorption band in the 280–380 nm range with maximum around 325 nm ($G \times \epsilon_{325} = 1.4 \times 10^{-3} \text{ dm}^3 \text{ J}^{-1} \text{ cm}^{-1}$; Figure 1A, curve a) and blue- and red-edge shoulders in 305–315 and 340–350 nm ranges, respectively. The 325-nm band formed within 5 μs after the pulse with $k_{\text{obs}} = (1.6 \pm 0.1) \times 10^6 \text{ s}^{-1}$. This apparent rate constant was proportional to the initial amount of peptide, which led to $k_4 = (8 \pm 1) \times 10^9 \text{ M}^{-1} \text{ s}^{-1}$ (Scheme 1). The 325-nm band decayed in biexponential mode within 1.2 ms after the pulse.

This spectrum should represent the combined absorption bands of hydroxycyclohexadienyl radicals of phenylalanine Phe($\cdot\text{OH}$) (**1b**) and of tyrosine Tyr(OH) (**1a**) (Scheme 1,

Scheme 1. First Steps of Oxidation of Leu-enk by $\cdot\text{OH}$ Radicals

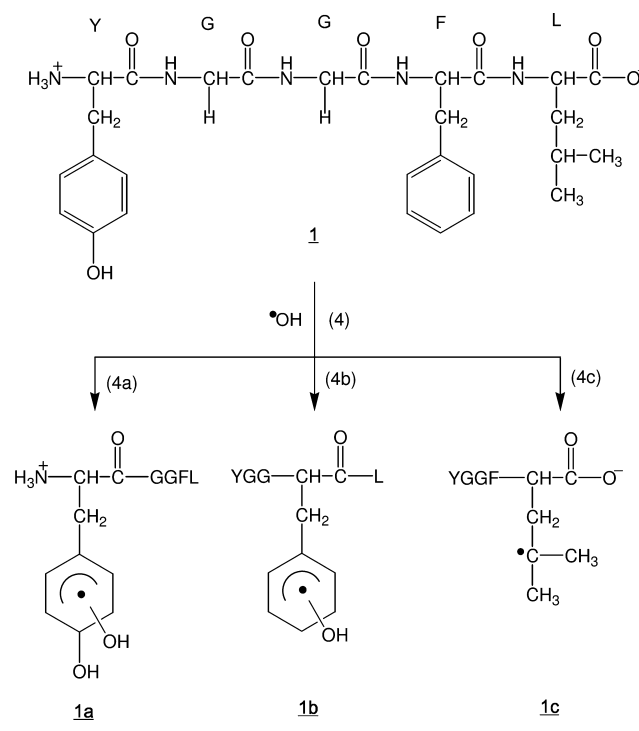


Figure S1, panels A and B, in the SI). It is noteworthy that, for this pH, an absorption band at 405 nm started to develop slowly within 150 μs after the pulse (Figure 1A, insert). However, its intensity was very weak. At 70 μs after the electron pulse, the spectrum in the range of 300–360 nm becomes less intense and much broader, with a more distinct shoulder located in the 300–315 nm range (Figure 1A, curve b). With the further elapse of time, the spectrum observed 140 μs after the pulse (Figure 1A, curve c) was blue-shifted and less intense characterized by a broad absorption band with weakly pronounced maximum around 320 nm. On the other hand, the absorption band with $\lambda_{\text{max}} = 405 \text{ nm}$ reached the plateau at 140 μs after the pulse, with $G \times \epsilon_{405} = 1.1 \times 10^{-4} \text{ dm}^3 \text{ J}^{-1} \text{ cm}^{-1}$ (Figure 1A, curve c).

Resolution of Transient Absorption Spectra. It was not possible to follow the transients directly from the raw data because of the significant overlap of their absorption spectra. The experimental spectrum recorded 5 μs after the pulse (Figure 1A, curve a) could be resolved into contributions from two components: **1a** and **1b** (Scheme 1, Figure S1 panel A, in the SI). The G values are reported in Table 1.

The sum over two component spectra with their respective yields ($G_{\text{total}} = 0.49 \mu\text{mol J}^{-1}$) is in reasonably good agreement with the expected yield of $\cdot\text{OH}$ radicals ($G_{\text{OH}} = 0.56 \mu\text{mol J}^{-1}$). It is lower than the initial yield of their precursor because the radicals derived from leucine (Leu) have not been taken into account. These C-centered radicals (reaction 4c, Scheme 1) do not absorb substantially at wavelengths $>290 \text{ nm}$. The calculated $G(\mathbf{1c}) = 0.07 \mu\text{mol J}^{-1}$ (Table 1), taken as a difference between G_{OH} and $G(\mathbf{1a} + \mathbf{1b})$, is in line with the lower rate constant of $\cdot\text{OH}$ radicals with Leu in comparison with the rate constants with Tyr and Phe.

The experimental spectrum recorded 140 μs after the pulse (Figure 1A, curve c) was best resolved into contributions from the same components as for the previous spectrum with $G(\mathbf{1a})$

Table 1. Primary Yields of the Free Radicals Resulting from \bullet OH Radical Attack on the Main Residue Targets in Leu Enkephalin^a

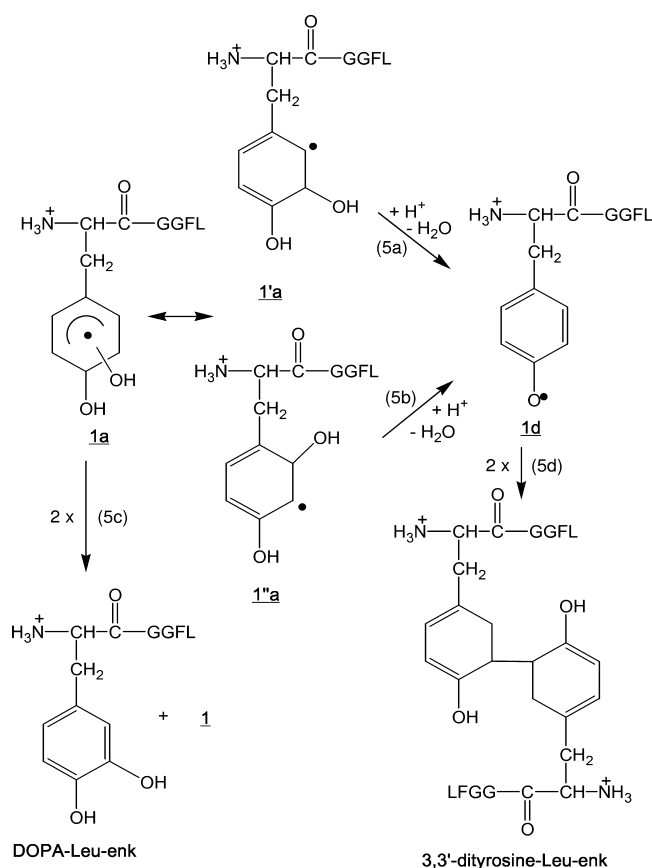
| residue | calc [a] (%) | exptl [b] (natural pH) | exptl [b] (pH 1) |
|---------------|--------------|------------------------|------------------|
| tyrosine | 61 | 0.39 (70) | 0.19 (68) |
| phenylalanine | 31 | 0.10 (18) | [c] |
| leucine | 8 | 0.07 (12) | [d] |
| Phe + Leu | 39 | (30) | (32) |

^a[a]: Percentages based on the rate constants with individual amino acids;²⁶ [b] yields ($\mu\text{mol J}^{-1}$), 5 μs after the pulse (in parentheses: % distribution of the OH yield); [c] determination not possible since the transient absorption spectra of **1b** and Phe(\bullet H) are very similar; [d] determination not possible since both \bullet OH and \bullet H are precursors of **1c** and **1c** does not absorb at wavelengths >290 nm. It is important to note that contribution of tyrosyl radicals (**1d**, Scheme 2) was negligible.

= 0.25 $\mu\text{mol J}^{-1}$ and $G(\mathbf{1b}) = 0.10 \mu\text{mol J}^{-1}$. Importantly, in contrast to the picture obtained at 5 μs , the fit of experimental results required contribution of tyrosyl radicals with $G(\mathbf{1d}) = 0.03 \mu\text{mol J}^{-1}$ (Scheme 2, Figure S1 panel B, in the SI).

Concentration Profiles of Transients. Resolutions of absorption spectra at any desired time delay following the electron pulse were performed in order to extract concentration profiles of **1a** and **1b** (Figure S1, panel C in the SI). The

Scheme 2. Reaction Steps of Dihydroxycyclohexadienyl Radicals of Tyr **1a** Residue in Leu-enk Leading to the Final Products



efficiency of transformation of **1a** radicals into **1d** was of particular concern. Taking the respective G values extracted at 5 and 140 μs , one could calculate that within 135 μs time window, the yield of **1a** radicals decreases by 0.14 $\mu\text{mol J}^{-1}$, whereas that of **1d** radicals increases only by 0.03 $\mu\text{mol J}^{-1}$. It shows that decay of **1a** radicals did not lead quantitatively to formation of **1d** radicals and strongly pointed out for another reaction pathway of decay of **1a** at pH 6.5, probably the disproportionation of the hydroxylated radicals (**1a**) leading to the final product DOPA-Leu-enk (reaction 5c, Scheme 2).

pH 1.0. UV-vis Transient Absorption Spectra. A transient spectrum obtained 5 μs after the electron pulse in N_2O -saturated solutions containing 0.2 mM of Leu-enk at pH 1.0, showed a broad absorption band in the 280–380 nm range with two weakly pronounced maxima at $\lambda_{\text{max}} = 305$ and 325 nm with $G\epsilon_{305} = 1.7 \times 10^{-3} \text{ dm}^3 \text{ J}^{-1} \text{ cm}^{-1}$ and $G\epsilon_{325} = 1.8 \times 10^{-3} \text{ dm}^3 \text{ J}^{-1} \text{ cm}^{-1}$ (Figure 1B, curve a) and some less defined absorptions below 300 nm toward UV. Contrary to what was observed at pH 6.5 (Figure 1A), the spectrum exhibits a third absorption band with two maxima at $\lambda_{\text{max}} = 390$ and 405 nm with $G\epsilon_{390} = 4.5 \times 10^{-4} \text{ dm}^3 \text{ J}^{-1} \text{ cm}^{-1}$ and $G\epsilon_{405} = 5.1 \times 10^{-4} \text{ dm}^3 \text{ J}^{-1} \text{ cm}^{-1}$ (Figure 1B, curve a).

The spectrum in the range of 305–350 nm became less intense and much broader, 70 μs after the electron pulse, with two pronounced maxima at 295 and 325 nm with $G\epsilon_{295} = 1.7 \times 10^{-3} \text{ dm}^3 \text{ J}^{-1} \text{ cm}^{-1}$ and $G\epsilon_{325} = 1.6 \times 10^{-3} \text{ dm}^3 \text{ J}^{-1} \text{ cm}^{-1}$, more intense less defined absorptions below 300 nm toward UV, and a more distinct shoulder located in the 345–355 nm range (Figure 1B, curve b). Moreover, the absorption bands at 390 and 405 nm continued further slow growth (Figure 1B, insert). 140 μs after the pulse, it became less intense in the range of 285–370 nm (Figure 1B, curve c). On the other hand, the absorption bands at 390 and 405 nm reached the plateau with $G\epsilon_{390} = 5.3 \times 10^{-4} \text{ dm}^3 \text{ J}^{-1} \text{ cm}^{-1}$ and $G\epsilon_{405} = 6.5 \times 10^{-4} \text{ dm}^3 \text{ J}^{-1} \text{ cm}^{-1}$ (Figure 1B, curve c).

Resolution of Transient Absorption Spectra. At pH 1, the hydrated electrons are converted into H atoms (reaction 3; see the Radiolysis of Water section), thus increasing $G(\bullet\text{H})$ from 0.06 to 0.34 $\mu\text{mol J}^{-1}$ and simultaneously decreasing $G(\bullet\text{OH})$ from 0.56 to 0.28 $\mu\text{mol J}^{-1}$. Therefore, the contribution of the cyclohexadienyl radicals Phe(\bullet H) and Tyr(\bullet H) to the absorption spectrum could not be neglected, in particular, in the 320–370 nm range (vide infra). The spectrum recorded represents the combined absorption bands of **1a**, **1b** and **1d** (Scheme 1, Figure S2, panel A in SI). It was only possible to estimate the sum of the radiation chemical yields of **1b** and cyclohexadienyl Phe(\bullet H) radicals in Phe since their spectral parameters (λ_{max} and ϵ) are very similar.³² Thus the experimental spectrum recorded 5 μs after the pulse (Figure 1B, curve a) could be resolved into contributions from four components: **1b** and Phe(\bullet H), with $G(\mathbf{1b}) + G(\text{Phe}(\bullet\text{H})) = 0.24 \mu\text{mol J}^{-1}$, the cyclohexadienyl radical in tyrosine Tyr(\bullet H), with $G(\text{Tyr}(\bullet\text{H})) = 0.16 \mu\text{mol J}^{-1}$, and **1d**, with $G(\mathbf{1d}) = 0.14 \mu\text{mol J}^{-1}$ (Figure S2, panel A, in the SI). Interestingly, the contribution of **1a** was found negligible. The sum over four component spectra with their respective yields ($G_{\text{total}} = 0.54 \mu\text{mol J}^{-1}$) is in reasonably good agreement with the sum ($G_{\text{total}} = 0.62 \mu\text{mol J}^{-1}$) of the expected yield of $\bullet\text{OH}$ radicals ($G_{\text{OH}} = 0.28 \mu\text{mol J}^{-1}$) and $\bullet\text{H}$ atoms ($G_{\text{H}} = 0.34 \mu\text{mol J}^{-1}$) at pH 1. The fact that combined yields of transients are lower than the initial yields of their precursors might be again due to the fact that in the resolution procedure the radicals derived from leucine (**1c**) have not been taken into account. The calculated $G(\mathbf{1c}) = 0.08 \mu\text{mol J}^{-1}$,

taken as a difference between $G_{\text{OH}+\text{H}}$ and a sum of $G(\mathbf{1d}) + \text{Tyr}(\bullet\text{H}) + (\mathbf{1b}) + \text{Phe}(\bullet\text{H})$ is in an excellent agreement with $G(\text{Leu}\bullet)$ calculated for pH 6.4 (vide supra).

The experimental spectrum recorded 140 μs after the pulse (Figure 1B, curve c) was best resolved into contributions from the same components as for the previous spectrum with $G(\mathbf{1b}) + G(\text{Phe}(\bullet\text{H})) = 0.19 \mu\text{mol J}^{-1}$, the cyclohexadienyl radical in tyrosine ($\text{Tyr}(\bullet\text{H})$, with $G(\text{Tyr}(\bullet\text{H})) = 0.12 \mu\text{mol J}^{-1}$, and $\mathbf{1d}$, with $G(\mathbf{1d}) = 0.19 \mu\text{mol J}^{-1}$ (Figure S2, panel B, in the SI). The sum of radiation chemical yields of cyclohexadienyl radicals $G(\text{Phe}(\bullet\text{H}) + \text{Tyr}(\bullet\text{H})) \geq 0.31 \mu\text{mol J}^{-1}$ is in a very good agreement with the expected radiation chemical yield of their precursor $G(\bullet\text{H}) = 0.34 \mu\text{mol J}^{-1}$.

Indirect determination of the initial yield of $\mathbf{1a}$ was possible. Indeed, one might expect that the final radiation chemical yield of $\mathbf{1d}$ radicals ($0.19 \mu\text{mol J}^{-1}$, measured 140 μs after the pulse) is equal to the primary radiation chemical yield of $\mathbf{1a}$. Taking that value, one might estimate the primary radiation chemical yield of $\mathbf{1b}$ as $G(\mathbf{1b}) \leq 0.09 \mu\text{mol J}^{-1}$ and simultaneously the primary radiation chemical yield of cyclohexadienyl radicals in phenylalanine $\text{Phe}(\bullet\text{H})$ as $G(\text{Phe}(\bullet\text{H})) \geq 0.15 \mu\text{mol J}^{-1}$ (Figure S2B, in the SI).

Concentration Profiles of Transients. Resolutions of absorption spectra at any desired time delay following the electron pulse were performed in order to extract concentration profiles of $\mathbf{1b}$, ($\text{Phe}(\bullet\text{H})$) derived from Phe, ($\text{Tyr}(\bullet\text{H})$), and $\mathbf{1d}$ (Figure S2, panel C in the SI). Taking the respective G values of $\mathbf{1d}$ radicals extracted at 5 and 140 μs , one can calculate that within 135 μs time window, the yield of $\mathbf{1d}$ radicals increased by $0.05 \mu\text{mol J}^{-1}$.

Kinetics of $\text{TyrO}\bullet$ Formation. The formation of the 405-nm absorption band showed pH-dependent biexponential kinetics after the electron pulse. From the mechanistic point of view, this points out that formation of $\mathbf{1d}$ radicals occurs via two independent processes. The plot of apparent rate constants against $[\text{H}^+]$ shows reasonably good straight lines with the slopes representing the respective bimolecular rate constants ($k_{\text{Sa}} = 1.7 \times 10^6 \text{ M}^{-1} \text{ s}^{-1}$; $k_{\text{Sb}} = 1.6 \times 10^7 \text{ M}^{-1} \text{ s}^{-1}$; Figure S3 in the SI) for the formation of $\mathbf{1d}$ via proton-catalyzed dehydration (reactions 5a and 5b, Scheme 2) of the respective two isomers $\mathbf{1}'\text{a}$ and $\mathbf{1}''\text{a}$.

Leu-Enkephalin: Final Products. UV-vis. γ -irradiated N_2O -saturated aqueous solutions containing Leu-enk (0.5 mM) at pH 6.5 exhibit three absorption bands located at 230, 277, and 290 nm and a weak shoulder in the range of 310–330 nm (Figure 2A). The intensity of these absorption bands increased linearly with the dose applied. The small peaks around 277 nm are reminiscent of 2,3-DOPA-Leu-enkephalin.³³ The absorption band at 290 nm and a shoulder in the range of 310–330 nm could be assigned to bityrosine of Leu-enkephalin.³⁴

HPLC. Leu-enk was irradiated with a dose of 90 Gy in N_2O -saturated aqueous solutions at pH 6.5. There was no fluorescence at 425 nm in the nonirradiated peptide, as expected (Figure 3A). The peak that was eluted at 17.5 min belongs to the native Leu-enk as shown in Figure 3A. Six products were formed after γ irradiation (Figure 3B,C). Only the compound with the elution time $t = 20.0$ min, fluoresced at 425 nm. It was assigned to a Leu-enk dimer linked by bityrosine.

Mass Spectrometry. Mass spectrometry analysis of irradiated samples showed that the major compounds corresponded to hydroxylated peptides. Gas phase fragmentation sequencing of the peptides revealed that both residues Tyr and Phe

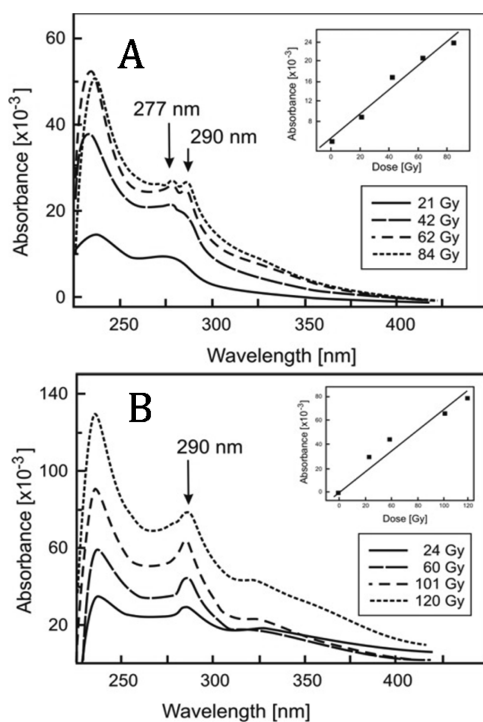


Figure 2. UV-visible difference absorption spectra (reference = non irradiated solution) recorded in γ -irradiated N_2O -saturated aqueous solutions. A: Leu-enk (0.5 mM) at pH 6.5. Insert: Change of the intensity of the absorption band at 290 nm with the dose. B: Met-Enk (0.5 mM) at pH 6.5. Insert: Change of the intensity of the absorption band at 290 nm with the dose.

underwent hydroxylation. Indeed, oxidation products of Tyr were detected as part of the b series fragments (B1 and B4).²⁸ Similarly, oxidation products of Phe were detected as part of the γ series (fragments $\gamma 2$ to $\gamma 4$). Increasing the dose allowed us to oxidize the peptide as much as 5 times, with detected species corresponding to the initial peptide plus up to five OH groups added to it. As first seen with HPLC, peptide dimers were detected. (Figure S4, panel D, in the SI). The relative amount of dimer with respect to the Leu-enk monomer was plotted vs dose (Figure 4). Interestingly, the amount of dimer was doubled by decreasing the pH of solutions from 6.5 to 1.

Met-Enkephalin: Transient Species. The reaction of $\bullet\text{OH}$ radicals with Met-enk was investigated in N_2O -saturated solutions over the concentration range of 0.1–0.6 mM, at various pH values.

Natural pH. UV-vis Transient Absorption Spectra. A transient absorption spectrum obtained 4 μs after electron pulse in N_2O -saturated aqueous solutions containing 0.1 mM of Met-enk at natural pH (pH 6.0) exhibits broad absorption bands in the 260–450 nm range with four distinct absorption maxima located at 295, 320, 390, and 405 nm, a shoulder around 350 nm, and some less defined absorption below 300 nm toward UV (Figure 5A, curve a). The respective $G\epsilon$ values are $G\epsilon_{295} = 1.5 \times 10^{-3}$, $G\epsilon_{320} = 1.25 \times 10^{-3}$, $G\epsilon_{390} = 4.3 \times 10^{-4}$, and $G\epsilon_{405} = 5.5 \times 10^{-4} \text{ dm}^3 \text{ mol}^{-1} \text{ cm}^{-1}$ (Figure 5A, curve a). It is noteworthy that the 405-nm band was fully developed 4 μs after the pulse (Figure 5A, insert), which is different from that observed at the same conditions for Leu-enk (vide Figure 1A, and insert).

The 320-nm band formed within 4 μs after the pulse with $k_{\text{obs}} = (1.5 \pm 0.1) \times 10^6 \text{ s}^{-1}$ (Figure 5A, insert). The spectra

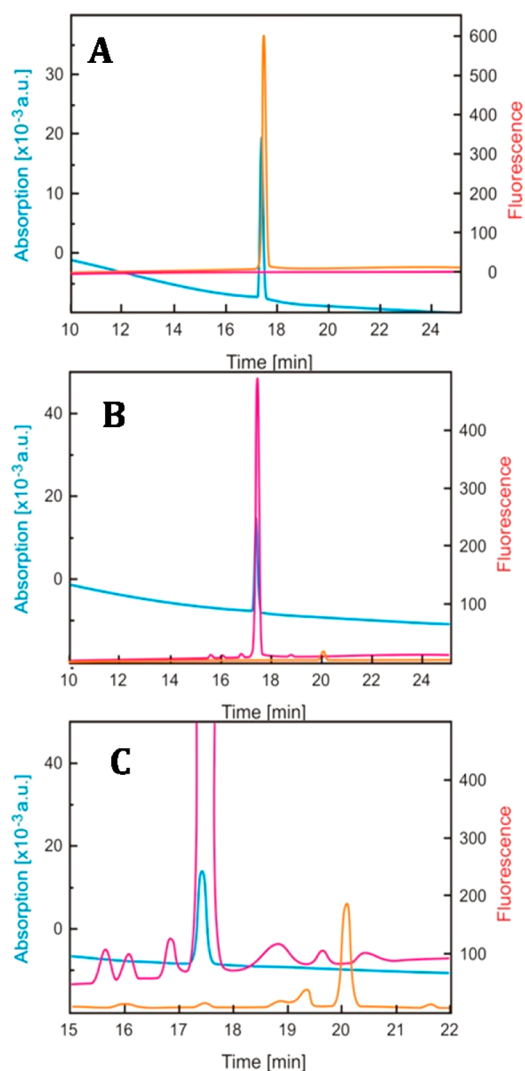


Figure 3. HPLC chromatograms of nonirradiated (panel A) and irradiated with 90 Gy (panels B and C) aqueous solutions containing Leu-enk (0.25 mM) at pH 6.5 saturated with N_2O . Absorption detection at 284 nm (blue line, left axis). Fluorescence detections with excitation at 284 nm and emission at 305 nm (magenta line, right axis) and 425 nm (orange line, right axis). For the panel C, the units of right y axis have been multiplied by 10.

recorded at 70 and 140 μs after the pulse exhibited similar features to that recorded at 4 μs except that absorption intensities in the range of 260–370 nm were lower whereas that located at 390 and 405 nm remained almost constant (Figure 5, curves b and c). Moreover, a peak with absorption maximum at 320 nm was now as a shoulder, and in the opposite, a shoulder around 350 nm has been developed as a weak peak.

The characteristic peaks at 390–405 nm resemble those of the tyrosyl radical³⁵ (**2d**). It suggests that, with Met-enk, **2d** is formed through a process that is not possible in Leu-enk. As the only difference with Leu-enk is the presence of a methionine instead of a leucine residue, it led us to assume that this new process for the formation of **2d** should involve a precursor resulted from a reaction between Met and the $\bullet OH$ radical.³⁶

Resolution of Transient Absorption Spectra. For the same reason as for Leu-enk at both pH's, the interpretation of the raw absorption spectra in the region of 280–450 nm is difficult. Moreover, in addition to five transients that could potentially

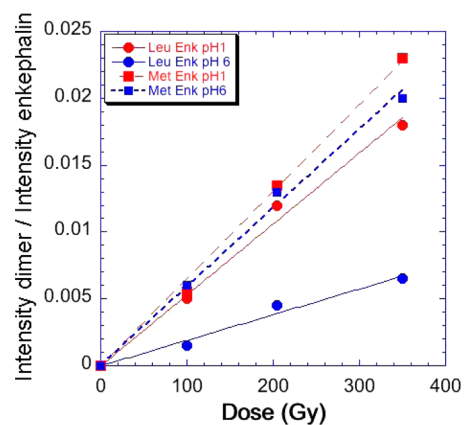


Figure 4. Ratio of the intensities of the m/z of the bityrosine derivative enkephalin on the m/z of the enkephalin versus the dose. Met-enk at pH 1.5 (red square), Met-enk at natural pH (blue square), Leu-enk at pH 1.5 (red circle), Leu-enk at natural pH (blue circle).

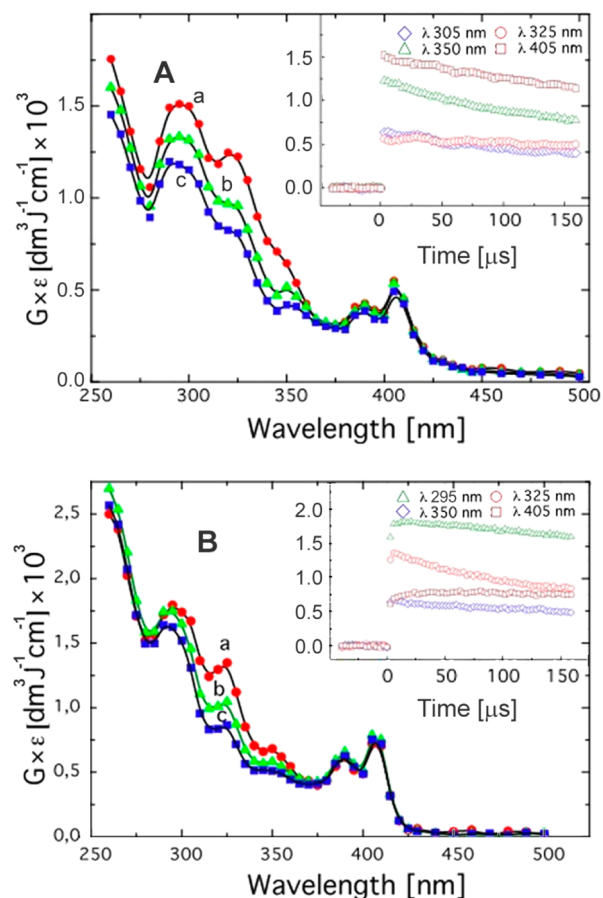
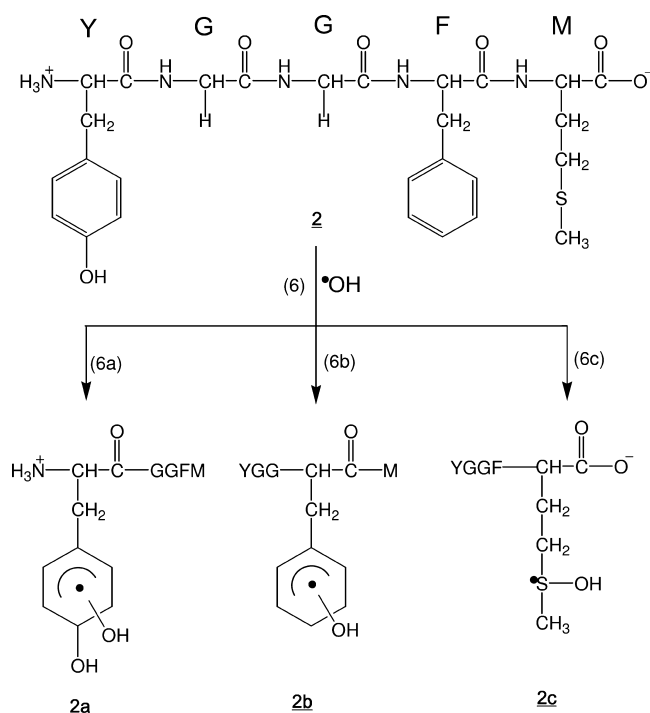
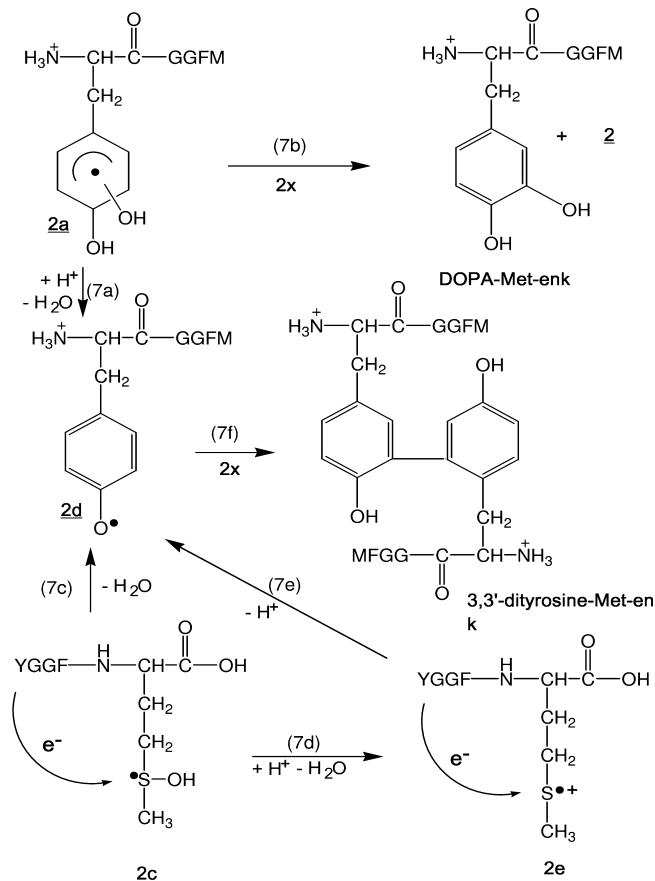


Figure 5. A: Transient absorption spectra recorded after electron pulse irradiation of an N_2O -saturated solution containing Met-enk (0.2 mM) at pH 6.0 with time delay: 4 μs (a, red circle), 70 μs (b, green triangle), and 140 μs (c, blue square). Insets: Kinetic traces recorded at 305, 320, 350, and 405 nm. B: Transient absorption spectra recorded after electron pulse irradiation of an N_2O -saturated solution containing Met-enk (0.2 mM) at pH 1.0 with time delay: 6 μs (a, red circle), 70 μs (b, green triangle), and 140 μs (c, blue square). Insets: Kinetic traces recorded at 305, 320, 350, and 405 nm.

contribute to this part of the spectrum [**2a** and **2b** (Schemes 3 and 4), two cyclohexadienyl radicals (Phe($\bullet H$), Tyr($\bullet H$)), and tyrosyl radical **2d** (Scheme 4)], one might expect transients

Scheme 3. First Steps of Oxidation of Met-enk by $\bullet\text{OH}$ RadicalsScheme 4. Reaction Steps of Dihydroxycyclohexadienyl Radicals of Tyr **2a** Residue and Hydroxysulfuranyl Radicals of Met Residue **2c** in Met-enk Leading to the Final Products

derived from Met residue. There are six potential species which might be formed upon oxidation of methionine by $\bullet\text{OH}$ radicals: hydroxysulfuranyl radicals ($\text{Met}(>\text{S}\bullet\text{-OH})$) (**2c**), intramolecularly three-electron-bonded $\text{S}\cdot\text{O}$ and $\text{S}\cdot\text{N}$ radicals, intermolecularly three-electron-bonded $\text{S}\cdot\text{S}$ dimeric radical cations, monomeric radical cations ($\text{MetS}^{\bullet+}$) (**2e**), and α -(alkylthio)-alkyl radicals ($\text{Met}(\alpha\text{S}\bullet)$).^{36a,37} All of them absorb in the region of 280–450 nm and could contribute to the experimental spectrum. The contribution of radicals coming from the reactions of H atoms were neglected as explained above.

The experimental spectrum recorded 4 μs after the pulse (Figure 5A, curve a) could be resolved into contributions from three components: **2a** and **2d** from Tyr and **2b** from Phe (Schemes 3 and 4, Figure S5, panel A, in the SI). The respective yields of each transient are collected in Table 2.

Table 2. Primary Yields of the Free Radicals Resulting from $\bullet\text{OH}$ Radical Attack on the Main Residue Targets in Met Enkephalin^a

| residue | calc [a] (%) | exptl [b] (natural pH) | exptl [b] (pH 1) |
|---------------|--------------|---|------------------|
| tyrosine | 41 | 0.31(2a) + 0.21 (2d) (57) | [c] |
| phenylalanine | 21 | 0.09 (17) | 0.04 (14) |
| methionine | 38 | 0.14 (26) | [c] |
| Tyr+Met | 79 | (83) | (86) |

^a[a] Percentages based on the rate constants with individual amino acids; [b] yields in $\mu\text{mol J}^{-1}$; [c] both Tyr(OH) and $\text{MetS}^{\bullet+}$ are precursors.

The sum over three component spectra ($G_{\text{total}} = 0.54 \mu\text{mol J}^{-1}$) is in very good agreement with the expected yield of $\bullet\text{OH}$ radicals ($G_{\text{OH}} = 0.56 \mu\text{mol J}^{-1}$). Moreover, there is no contribution of Met-derived radicals (**2c** and derivatives). The initial concentration of the transient species (**2c**; $0.14 \mu\text{mol J}^{-1}$) was calculated indirectly and taken as the concentration of tyrosyl radicals (**2d**) measured 4 μs after the pulse (Figure S5A, in the SI).

The experimental spectrum recorded 140 μs after the pulse (Figure 5A, curve c) was best resolved into contributions from the same components as for the previous spectrum with $G(\mathbf{2a}) = 0.18 \mu\text{mol J}^{-1}$, $G(\mathbf{2b}) = 0.08 \mu\text{mol J}^{-1}$, and $G(\mathbf{2d}) = 0.14 \mu\text{mol J}^{-1}$.

Concentration Profiles of Transients at Natural pH. Panel C in Figure S4 shows radiation chemical yield (G) versus time plots for the three intermediates **2a**, **2b**, and **2d**. On the basis of extracted concentration profiles, it was possible to conclude whether the apparent decay of **2a** occurs with accompanying formation of **2d** (reaction 7a, Scheme 4). Taking the respective G values extracted at 4 and 140 μs , one can simply calculate that, within the 136 μs time window, the yield of **2a** decreases by $0.13 \mu\text{mol J}^{-1}$, whereas the yield of **2d** remains constant. From the mechanistic point of view, this shows that decay of **2a** does not lead quantitatively to formation of **2d** radicals and strongly points out for another reaction pathway of decay of **2a**, possibly leading to DOPA-Met-enk (reaction 7b, Scheme 4).

pH 1. UV-vis Transient Absorption Spectra. A transient absorption spectrum obtained 4 μs after electron pulse in N_2O -saturated aqueous solutions containing 0.2 mM of Met-enk at pH 1.0, exhibited broad absorption bands in the 270–450 nm

range with five distinct maxima (295, 325, 350, 390, and 405 nm; Figure 5B, curve a; $G_{\epsilon_{295}} = 1.8 \times 10^{-3}$, $G_{\epsilon_{325}} = 1.4 \times 10^{-3}$, $G_{\epsilon_{350}} = 6.8 \times 10^{-4}$, $G_{\epsilon_{390}} = 6.2 \times 10^{-4}$, $G_{\epsilon_{405}} = 7.2 \times 10^{-4}$ dm³ mol⁻¹ cm⁻¹; Figure 5B, curve a). The 320-nm band formed within 4 μ s after the pulse with $k_{\text{obs}} = (1.5 \pm 0.1) \times 10^6$ s⁻¹ (Figure 5B, insert). Again the bands at 390–405 nm were developed within 4 μ s after the pulse (Figure 5B curve a, insert). The spectra recorded at 70 and 140 μ s after the pulse exhibited similar features to those recorded at 4 μ s except that absorption intensities in the range of 260–370 nm were lower whereas those located at 390–405 nm slightly increased (Figure 5B, curves b and c).

Resolution of Transient Absorption Spectra. The contribution of the cyclohexadienyl radicals Phe[•]H and Tyr[•]H to the absorption spectrum cannot be neglected, in particular, in the 320–370 nm range (vide supra). The spectrum should thus represent the combined absorption bands of **2b** (Scheme 3), Tyr[•](H) and phenylalanine Phe[•](H), and **2d** (Scheme 4) (Figure S6, panels A and B, in the SI).

From the spectral resolutions, it was only possible to estimate the sum of the radiation chemical yields of **2b** and Phe[•](H) radicals since their spectral parameters (λ_{max} and ϵ) are very similar (vide supra). Taking this into account, the experimental spectrum recorded 4 μ s after the pulse (Figure 5B, curve a) could be resolved into contributions from four components: **2b** and Phe[•](H), with $G(\mathbf{2b}) + G(\text{Phe}^{\bullet}(\text{H})) = 0.18 \mu\text{mol J}^{-1}$, (Tyr[•](H), with $G(\text{Tyr}^{\bullet}(\text{H})) = 0.11 \mu\text{mol J}^{-1}$, and **2d** with $G(\mathbf{2d}) = 0.21 \mu\text{mol J}^{-1}$ (Figure S6, panel A, in the SI). Again the sum over four component spectra with their respective yields ($G_{\text{total}} = 0.52 \mu\text{mol J}^{-1}$) is lower than the sum (of the expected yield of [•]OH radicals and [•]H atoms ($G_{\text{OH}} + G_{\text{H}} = 0.28 + 0.34 = 0.62 \mu\text{mol J}^{-1}$). It might be due to the fact that the absorption spectrum of CH₃S[•] from the H-atom reaction with Met has not been taken into account.

The experimental spectrum recorded 140 μ s after the pulse (Figure 5B, curve c) was best resolved into contributions from the same components as for the previous spectrum with $G(\mathbf{2b}) + G(\text{Phe}^{\bullet}(\text{H})) = 0.11 \mu\text{mol J}^{-1}$, the cyclohexadienyl radical in Tyr (Tyr[•](H), with $G(\text{Tyr}^{\bullet}(\text{H})) = 0.08 \mu\text{mol J}^{-1}$, and the tyrosyl radical **2d**, with $G(\mathbf{2d}) = 0.24 \mu\text{mol J}^{-1}$ (Figure S6, panel B, in the SI). For pH 1, one might expect that the final radiation chemical yield of **2d** ($0.24 \mu\text{mol J}^{-1}$) is equal to the sum of the primary radiation chemical yields of **2a** and **2c**. Taking that value, one might estimate the primary radiation chemical yield of **2b**: $G(\mathbf{2b}) = 0.04 \mu\text{mol J}^{-1}$. This value allows calculation of the primary radiation chemical yield of cyclohexadienyl radicals in phenylalanine (Phe[•](H)): $G(\text{Phe}^{\bullet}(\text{H})) = 0.14 \mu\text{mol J}^{-1}$. The sum of radiation chemical yields of cyclohexadienyl radicals $G(\text{Phe}^{\bullet}(\text{H}))$ and $G(\text{Tyr}^{\bullet}(\text{H})) = 0.25 \mu\text{mol J}^{-1}$ is lower than the radiation chemical yield of their precursor $G(^{\bullet}\text{H}) = 0.34 \mu\text{mol J}^{-1}$. Indeed the absorption spectrum of thiyl radicals (CH₃S[•]) derived from Met and formed with $G(\text{CH}_3\text{S}^{\bullet}) = 0.09 \mu\text{mol J}^{-1}$ has not been taken into account.³⁸

Concentration Profiles of Transients. Resolutions of absorption spectra at any desired time delay following the electron pulse were performed in order to extract concentration profiles of **2b** and Phe[•](H) derived from Phe, Tyr[•](H) and **2d**. Radiation chemical yields (G) versus time plot for these transients are shown in Figure S6, panel C (in the SI). Taking the respective G values of **2d** extracted at 6 and 140 μ s, one can calculate that within 134 μ s time window, the yield of **2d**

radicals increased by $0.03 \mu\text{mol J}^{-1}$. It points out that formation of **2d** occurs via two independent processes (vide infra).

The apparent first order rate constants at 325 and 405 nm were proportional to the initial concentration of Met-**enk**, hence rate constants k_6 equal to $(1.16 \pm 0.1) \times 10^{10} \text{ M}^{-1} \text{ s}^{-1}$ and $(1.36 \pm 0.2) \times 10^{10} \text{ M}^{-1} \text{ s}^{-1}$ were deduced (Scheme 3). Their similarity points out that formation of TyrO[•] radicals is not controlled by the intramolecular transformation involving radical transients derived from Met residue.

Met-Enkephalin: Final Products. *UV-vis.* Met-**enk** (0.5 mM) was irradiated in N₂O-saturated aqueous solutions at natural pH (ca. 6.0) with several doses in the range of 20–120 Gy (Figure 2B). The absorption band at 290 nm increased linearly with the dose. (Figure 2B, insert). Contrary to the N₂O-saturated solution containing Leu-**enk** (Figure 2A) no small peak with λ_{max} around 277 nm was observed. Conversely, the absorbance around 320 nm and up to the visible region increased with the dose. Taken together, it indicates the formation of dityrosines.

HPLC. Three peaks with elution times 16.8 min, 18.6 and 19.6 min were observed after γ -irradiation (Figure S7, in the SI). The peak eluting at 16.8 min observed in the nonirradiated sample was assigned to the native Met-**enk**. Two products represented by the peaks with elution times 18.6, and 19.6 min exhibited fluorescence at 425 nm. The peak eluted after 18.6 min and detected by the same fluorescence setting (ex: 284 nm, em: 425 nm) was characterized by the highest intensity emission at $\lambda = 425$ nm. Therefore its presence could be assigned to the formation of dityrosine of Met-**enk**,³⁴ in line with our earlier observations in solutions containing Met-**enk** and the N₃[•] radical as one-electron oxidant.²⁰ The product eluted after 19.6 min also exhibited a characteristic fluorescence at 425 nm and was tentatively assigned to another isomer of dityrosine of Met-**enk**.

Mass Spectrometry. Solutions of Met-**enk** were irradiated up to 900 Gy. Irradiation of the samples yielded a number of distinct molecular species: (i) oxidized species detected as mass increments of 16 Da on the monocharged ion, (ii) dimeric biprotonated at $m/z = 577.22$, and (iii) a molecular species corresponding to a loss of 47 Da from the YGGFM peptide. In all cases the mass peaks increased with the γ -irradiation dose (Figure 6 and Figures S8A and B, in the SI).

Each ion described above was fragmented in a gas phase. The ion at $m/z = 528.33$ (loss of 47 Da) corresponded to desulfurated methionine, also called aminobutyric acid (Aba). Its formation is attributed to the reactions of H atoms with methionine.³⁸ As expected this reaction is minor in solutions at natural pH but quite important in acidic medium. Fragmentation in a gas phase of the ions at $m/z = 590.22$ (increment of 16 Da) revealed that they correspond to a mixture of two hydroxylated peptides: at methionine (i.e., methionine sulfoxide) and at tyrosine (i.e., DOPA-Met-**enk**).

Interestingly, we found a very low amount of hydroxylated phenylalanine, contrary to what was observed in Leu-**enk**. In addition, for the highest dose, we also found doubly hydroxylated forms of Met **enk** corresponding to the presence of either methionine sulfone or a mixture of methionine sulfoxide and hydroxylated tyrosine (DOPA-Met-**enk**). As for the dimer, the ratio of intensities (dimer)/(Met-**enk**) did not vary with the pH from 1.5 to 6.5 (Figure 4).

Computational Analysis. The aim was to verify whether conformations of Met-**enk** exhibiting proximity between the sulfur atom of Met residue and the OH group of Tyr residue in

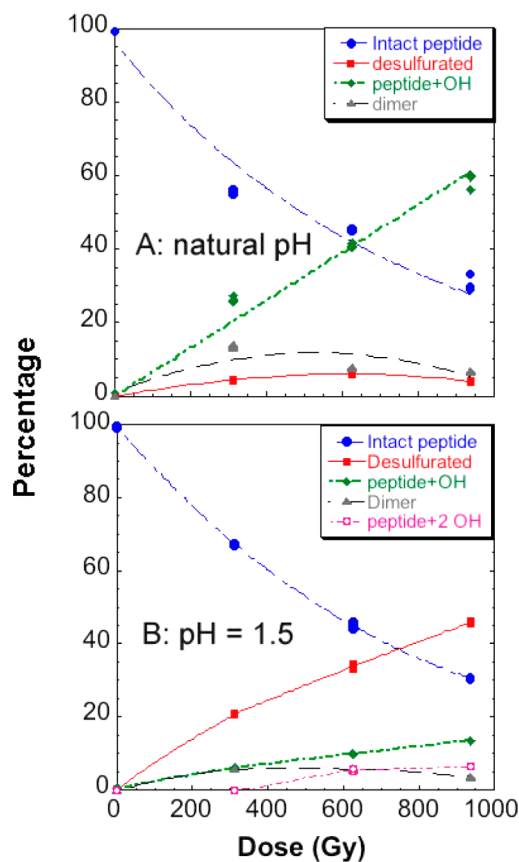


Figure 6. Variation of the relative intensity of the different final compounds formed after radiolysis of Met-enkephalin in N_2O -saturated solutions at natural pH and at pH 1.5.

water are stable enough, to allow very fast intramolecular electron transfer from Tyr residue to Met residue. A complete conformational analysis of this peptide was not performed since several papers dealing with this subject were published.³⁹ However, the question of the distance between the sulfur atom of Met and the $-OH$ group of Tyr ($S-O$) has never been addressed before.

We used a simple DFT approach (B3LYP/6-31G*) and the starting points were seven conformations among the ca. 80 ones deposited in the PDB (1PLW). It should be noted that these experimental structures were recorded in micelles and not in water, thus their stability in water can be questioned. The starting points were chosen for their different levels of folding. Among the fully optimized structures, two exhibited small $S-O$ distances (lower than 6 Å) in agreement with the very fast electron transfer observed by pulse radiolysis. Their energies were 3.83 and 6.90 kJ mol^{-1} higher than the most stable structure, indicating that both could be attained in solutions at room temperature. The structure of lowest energy is shown in Figure 7B with an experimental conformation in micellar environment (Figure 7A).

DISCUSSION

We have investigated the one-electron oxidation of both Leu- and Met-enkephalins by $\bullet OH$ radicals. These peptides contain major targets of reactive oxygen species, two aromatic residues (tyrosine and phenylalanine) and in Met-enk additionally one methionine residue. Our aims were to determine the kinetic process, to evaluate the proton-assisted steps in the

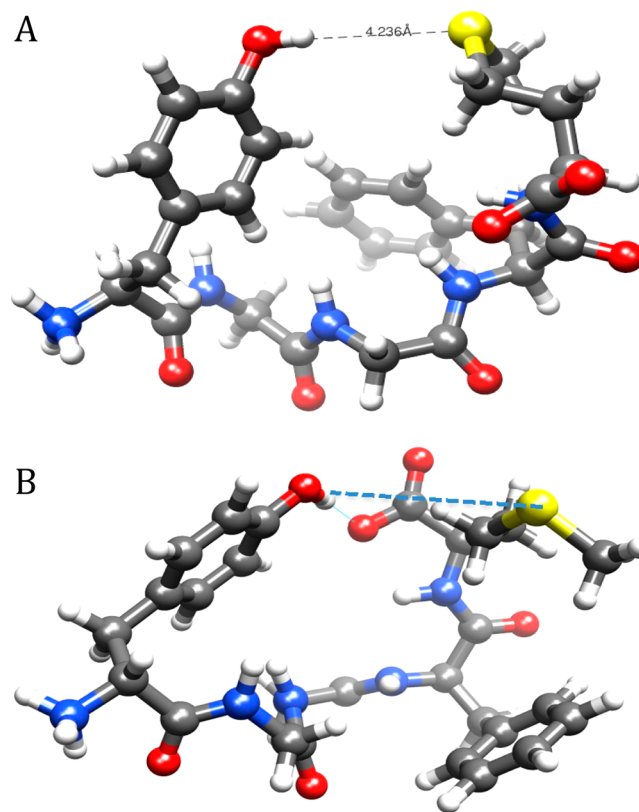


Figure 7. (A) Experimental conformation of Met-enk in micelles (PDB, 1PLW, structure 51). (B) Structure of lowest energy optimized in water (B3LYP/6-31G*). Both would be in agreement with a very fast intramolecular electron transfer between $MetS^{\bullet}OH/Met^{\bullet}$ and Tyr.

mechanisms of oxidation, the final products, and the influence of the sequence and pH on their nature.

Oxidation Mechanism in Leu-enk. Fast formation of OH adducts on both aromatic residues Tyr (**1a**) (reaction 4a, Scheme 1) and Phe (**1b**) in Leu-enk (reaction 4b, Scheme 1) ($k_4 = (8 \pm 1) 10^9 \text{ M}^{-1} \text{ s}^{-1}$) was confirmed unquestionably by pulse radiolysis. Resolution of transient absorption spectra at natural pH (Figure S1A, in the SI) allowed direct determination of their initial yields (Table 1) and thus primary distribution of the $\bullet OH$ attack (in %) on the main residue targets (Tyr and Phe) (Table 1, column 2). They follow the trend of those calculated by taking the rate constants of the $\bullet OH$ radical reactions with the respective individual amino acids (Table 1, column 1). However the one of **1b** (18%) is substantially lower to that calculated (31%). This observation is consistent with the already reported low amount of *o*- and *p*-tyrosine formed from the oxidation of Phe by $\bullet OH$ radicals (10% of the total $\bullet OH$ yield).⁴⁰

At pH 1 the primary distribution yield of the $\bullet OH$ radical attack on both Phe and Leu residues (32%) is similar to that for natural pH (30%) (Table 1, columns 2 and 3). The primary distribution yield of **1a** (68%) normalized to the total yield of $\bullet OH$ radicals ($0.28 \mu\text{mol J}^{-1}$) available at pH 1 is practically the same as that measured at natural pH (70%) (Table 1, columns 2 and 3).

It is well-known that $\bullet OH$ radicals form ortho and meta isomers of the dihydroxy-cyclohexadienyl radical adducts on the tyrosine ring, and an addition to the ortho position of the tyrosine ring is the most favorable.⁴¹ These isomers undergo

proton-catalyzed dehydration with different rate constants. Similarly, **1'a** and **1''a** underwent dehydration (reactions 5a and 5b, Scheme 2). Thus, the decay pathway of **1a** is controlled by a competition between disproportionation (reaction 5c, Scheme 2) and acid-catalyzed dehydration mechanisms (reactions 5a and 5b, Scheme 2).⁴² Consequently the amount of dimers linked by dityrosines was low in neutral medium and higher in acidic one (Figure 4). The final products resulting from the •OH attack on tyrosine in Leu-enk are mostly either DOPA-Leu-enk (reaction 5c, Scheme 2) in neutral and slightly acidic medium or dimers (3,3'-dityrosine-Leu-enk) in acidic medium (reaction 5d, Scheme 2).

Oxidation Mechanism in Met-enk. Fast formation of OH adducts on both aromatic residues Tyr (**2a**) (reaction 6a in Scheme 3) and Phe (**2b**) in Met-enk (reaction 6b, Scheme 3) ($k_6 = (1.3 \pm 0.1) 10^{10} \text{ M}^{-1} \text{ s}^{-1}$) was also confirmed by pulse radiolysis. However, no transient coming from methionine was observed (**2c** and/or **2e**).^{36a,43,37d,44}

Interestingly, a comparison of the absorption spectra of transients derived from Met-enk and Leu-enk recorded 4 μs after the pulse and at natural pH revealed a substantial difference (Figures 5A and 1A, respectively). The characteristic absorption band with $\lambda_{\text{max}} = 405 \text{ nm}$ of tyrosyl radical is clearly seen very fast with Met-enk (within 4 μs , Figure 5A, insert), and absent with Leu-enk albeit rate constants of reactions with •OH radicals are very close ($(8 \pm 1) 10^9$ and $(1.3 \pm 0.1) 10^{10} \text{ M}^{-1} \text{ s}^{-1}$ for Leu-enk and Met-enk, respectively). These observations led us to the hypothesis that TyrO• radical (**2d**) should be formed through a new process not present in Leu-enk, i.e. an electron transfer involving a hydroxysulfuranyl radical on Met residue (**2c**) and a Tyr residue (reaction 7c, Scheme 4). The reduction potential $E^0(\text{MetS}^\bullet\text{OH}/\text{MetS})$ is not known. Assuming a value similar to that of dimethylsulfide (DMS) (+1.41 V (vs NHE)⁴⁵) and $E^0(\text{TyrO}^\bullet, \text{H}^+/\text{TyrOH}) = +1.0 \text{ V}$ (vs. NHE)⁴⁶ at pH 6, it would be thermodynamically feasible.

Resolution of transient absorption spectra at natural pH (Figure S5A, in the SI) after pulse radiolysis of Met-enk solutions allowed direct determination of the initial concentration of the transient species (Table 2, column 2). As it was found for Leu-enk, the yields follow the trend of the rate constants of the •OH radical reactions with the respective individual amino acids (Table 2, column 1). However, the primary distribution yields of **2b** (17%) and **2c** (26%) normalized to the total yield of •OH radicals were substantially lower than those calculated (21%, 38%, respectively) taking the respective rate constants of •OH radicals with Phe and Met.

Transients **2a** and **2c** underwent at pH 1 proton-catalyzed dehydrations (reactions 7a and 7d, Scheme 4). Both processes led to **2d** within the same time window (less than 4 μs). The intramolecular electron transfer from Tyr to Met radical would be thermodynamically feasible on the basis of the reduction potential of DMS⁴⁵ and $E^0(\text{TyrO}^\bullet, \text{H}^+/\text{TyrOH}) = 1.3 \text{ V}$ (vs NHE)^{46,36b} at pH 1. Similar process was observed in Met-enk during photosensitized oxidation of Tyr and Met by the triplet state of 4-carboxybenzophenone.⁴⁷

Since both **2a** and **2c** were precursors of **2d**, a resolution of absorption spectra at pH 1 (Figure S6B, in the SI) after pulse radiolysis of Met-enk solutions did not allow even indirect determination of their initial concentrations. Thus, the primary distribution yield of the •OH attack (in %) could be only calculated for both residues (Met + Tyr) and was equal to 86% (Table 2, column 3). The last value allowed calculation of the

•OH attack probability on Phe residue equal to 14%, i.e. practically the same as that measured at natural pH (16%) (Table 2, columns 2 and 3).

Intramolecular Electron Transfer in Met-enk. Three questions arise which are directly connected with the postulated intramolecular electron transfer in Met-enk: (i) Can intermolecular electron transfer (ET) be neglected? (ii) What is the rate constant for intramolecular ET? (iii) What is the mechanism of intramolecular ET, does it occur through space (solvent) or through the peptide bonds?

The answer for the first question is the following: under experimental conditions (0.2 mM of Met-enk), intermolecular ET could be neglected. The rate constant for intermolecular electron transfer between $\text{Met}(\text{S}^\bullet\text{S})^+$ and Tyr ($k = 3.8 \times 10^7 \text{ M}^{-1} \text{ s}^{-1}$),⁴⁸ can only compete with intramolecular ET for very high concentrations of Met-enk (>0.1 M, vide infra).

The intramolecular ET step was not observed using the ELYSE picosecond pulse radiolysis set up.⁴⁹ Using the Met-enk initial concentration of 1.1 mM, the formation of **2d** (observed at 405 nm) was found to occur with $\tau_{1/2} \approx 60 \text{ ns}$ which corresponds to the pseudo-first order rate constant equal to $1.2 \times 10^7 \text{ s}^{-1}$. This observation increased the lower limit for the rate constant of intramolecular ET by nearly 1 order of magnitude. Dividing this value by a concentration of Met-enk used, one can arrive with the value of $\sim 1 \times 10^{10} \text{ M}^{-1} \text{ s}^{-1}$, which is very close to the k_6 value. In another words, formation of **2d** is controlled in principle by reaction 6 (Scheme 3), and not by reaction 7c (Scheme 4). A high value of the rate constant for intramolecular ET in Met-enk is consistent with the lack of α -(alkylthio)alkyl radicals in the resolution of transient absorption spectra and with the lack of CO₂ formation.⁵⁰ The former radical might be potentially produced by the competitive deprotonation of **2c** and **2e**. Formation of CO₂ would have resulted from the competitive oxidation of the carboxylate function in Met via intramolecular ET in **2c** and **2e** transients.⁵⁰

The difficulty in elucidating whether the intramolecular ET occurs through space or through the peptide bonds is due to the large variety of conformations in which the enkephalins can exist in aqueous environment. In the Protein Data Bank (PDB 1PLW) ca. 80 conformations of Met-enk in micelles were observed by NMR. Among them several show close proximity between these two residues. A typical structure (structure 51, PDB 1PLW) is shown in Figure 7A. Optimization with DFT methods taking into account solvation in water showed that conformations with a close proximity of the sulfur atom and the –OH group of tyrosine were stable in water at room temperature (Figure 7B). Calculations showed that in the radical cation of Met-enk the odd electron orbital was delocalized on the sulfur atom and on the tyrosine aromatic ring.⁵¹ Previous conformational analysis using Empirical Conformational Energy Program for Peptides (ECEPP) has shown existence of hydrogen bonds in the lowest energy structures of Met-enk. One of them having the length of 1.90 Å involves Tyr and Met residues.^{39c} A more recent molecular mechanics optimization (BIOS-CHARMM) has shown the existence of 4 hydrogen bonds in the optimized structure of Met-enk (type I'– β -bend). One of them involves the proton of the N-terminal amine group (in Tyr residue) and the oxygen atom in the carbonyl group located between Phe and Met residues.⁴⁹

Earlier oxidation studies of peptides containing Tyr and Met residues and Met-enk using $\text{Br}_2^{\bullet-}$ as a selective one-electron oxidant allowed determination of first-order rate constants of

intramolecular ET involving Met(S:Br) and Tyr residues ($1.1 \times 10^5 \text{ s}^{-1}$).⁵² Similar feature was observed when $\bullet\text{OH}$ radical was used for oxidation of Tyr-Met dipeptides. The lower limit for the rate constant of intramolecular ET was found to be $2.5 \times 10^6 \text{ s}^{-1}$.⁵³

On the other hand, the rate constant for intramolecular ET between Met(S:Br) and Tyr residues measured in Tyr-(Pro)₃-Met (a peptide having the same number (3) of amino acid residues between Tyr and Met residues as Met-enk) was found to decrease by 1 order of magnitude and equal to $1.1 \times 10^4 \text{ s}^{-1}$.⁵⁴ In this case intramolecular ET is likely partitioning along the peptide backbone and direct water mediated contacts between groups bearing radical sites.

Taking all these structural and experimental features above into account, one can suspect that most probably in Met-enk an intramolecular ET occurs rather through space (water) pathway with a possible involvement of the hydrogen bond shortcuts.

CONCLUSIONS

The oxidation of proteins is known to be a major event in many problems related to oxidative stress. After oxidation, the protein can be totally destabilized, and lose⁵⁵ or increase its activity.⁵⁶ Although a lot is known about protein oxidation still many facts are not understood.

In this work we have compared the oxidation processes of two pentapeptides differing only by their C-terminal residues. This difference had consequences in the oxidation process. In Leu-enk, the N-terminal residue became DOPA instead of tyrosine. In Met-enk, tyrosine dimers are created as a consequence of intramolecular electron transfer to methionine. It means that the fate of tyrosine in oxidative stress and thus the biomarkers coming from this residue can differ according to the protein sequence and the neighboring residues and the character of the oxidant.

Similar difficulties may concern other residues thus the story of protein oxidation is far from being completed.

ASSOCIATED CONTENT

Supporting Information

Resolution of the spectral components and their concentration profiles (Figures S1, S2, S5, and S6), variation of the rate constant vs pH for Leu enk (Figure S3), ES-MS spectra (Figures S4 and S8), and HPLC chromatograms (Figure S7) are included. This material is available free of charge via the Internet at <http://pubs.acs.org>.

AUTHOR INFORMATION

Corresponding Author

*E-mail: k.bobrowski@ichtj.waw.pl; Chantal.houee@u-psud.fr.

Notes

The authors declare no competing financial interest.

ACKNOWLEDGMENTS

We thank Dr. J.-L. Marignier for the use of the ELYSE ultra fast pulse radiolysis set up. The support and sponsorship of the COST Action CM0603 on "Free Radicals in Chemical Biology" (CHEMBIORADICAL), of the COST Action CM1001 "Non-enzymatic protein oxidation", and the financial help of the Non-Cofinancing International Project of the Polish Ministry of Science and Higher Education (455/N-COST/2009/0) are kindly acknowledged.

REFERENCES

- (1) Henry, B.; Duty, S.; Fox, S. H.; Crossman, A. R.; Brotchie, J. M. *Exp. Neurol.* **2003**, *183*, 458–468.
- (2) (a) Mathieu-Kia, A. M.; Fan, L. Q.; Kreek, M. J.; Simon, E. J.; Hiller, J. M. *Brain Res.* **2001**, *893*, 121–134. (b) Yew, D. T.; Li, W. P.; Webb, S. E.; Lai, H. W.; Zhang, L. *Exp. Gerontol.* **1999**, *34*, 117–133. (c) Rissler, D.; You, Z. B.; Cairns, N.; Herrera-Marschitz, M.; Seidl, R.; Schneider, C.; Terenius, L.; Lubec, G. *Neurosci. Lett.* **1996**, *203*, 111–114.
- (3) Grune, T.; Jung, T.; Merker, K.; Davies, K. J. A. *Int. J. Biochem. Cell Biol.* **2004**, *36*, 2519–2530.
- (4) Stryer, L. *Biochemistry*; W. H. Freeman and Company: New York, 1988.
- (5) Terenius, L.; Wahlstrom, A.; Lindeberg, G.; Karlsson, S.; Ragnarsson, U. *Biochem. Biophys. Res. Commun.* **1976**, *71*, 175–179.
- (6) Hughes, J.; Smith, T. W.; Kosterlitz, H. W.; Fothergill, L. A.; Morgan, B. A.; Morris, H. R. *Nature* **1975**, *258*, 577–579.
- (7) (a) Thanavala, V.; Kadam, V. J.; Ghosh, R. *Curr. Drug Targets* **2008**, *9*, 887–894. (b) Smith, H. S. *Pain Physician* **2008**, *11* (2 Suppl), S121–132. (c) Machelska, H. *Neuropeptides* **2007**, *41*, 355–363.
- (8) Papathanassoglou, E. D.; Giannakopoulou, M.; Mpouzika, M.; Bozas, E.; Karabinis, A. *Nurs. Crit. Care* **2010**, *15*, 204–216.
- (9) Sobocanec, S.; Balog, T.; Sverko, V.; Marotti, T. *Physiol. Res.* **2005**, *54*, 97–104.
- (10) Sobocanec, S.; Kusic, B.; Sverko, V.; Balog, T.; Marotti, T. *Biogerontology* **2006**, *7*, 53–62.
- (11) Balog, T.; Sobocanec, S.; Sverko, V.; Marotti, T. *Neuropeptides* **2004**, *38*, 298–303.
- (12) Plotnikoff, N. P.; Faith, R. E.; Murgo, A. J.; Herberman, R. B.; Good, R. A. *Clin. Immunol. Immunopathol.* **1997**, *82*, 93–101.
- (13) (a) Bolling, S. F.; Badhavar, V.; Schwartz, C. F.; Oeltgen, P. R.; Kilgore, K.; P., S. J. *Thorac. Cardiovasc. Surg.* **2001**, *122*, 476–481. (b) Plotnikoff, N. P.; Faith, R. E.; Murgo, A. J.; Good, R. A. *Enkephalins and Endorphins. Stress and Immune System*; Plenum Press: New York, 1986; pp 1–446.
- (14) Reichling, D. B.; Levine, J. D. *Ann. Neurol.* **2011**, *69*, 13–21.
- (15) Rosei, M. A.; Blarmino, C.; Foppoli, C.; Coccia, R.; De Marco, C. *Biochem. Biophys. Res. Commun.* **1991**, *179*, 147–152.
- (16) Rabgaoui, N.; Slaoui-Hasnaoui, A.; Torrelles, J. *Free Radic. Biol. Med.* **1993**, *14*, 519–529.
- (17) Fontana, M.; Mosca, L.; Rosei, M. A. *Biochem. Pharmacol.* **2001**, *61*, 1253–1257.
- (18) Coccia, R.; Foppoli, C.; Blarmino, C.; De Marco, C.; Rosei, M. A. *Biochim. Biophys. Acta* **2001**, *1525*, 43–49.
- (19) Fontana, M.; Pecci, L.; Schinina, M. E.; Montefoschi, G.; Rosei, M. A. *Free Radic. Res.* **2006**, *40*, 697–706.
- (20) Mozziconacci, O.; Mirkowski, J.; Rusconi, F.; Pernot, P.; Bobrowski, K.; Houée-Levin, C. *Free Radical Biol. Med.* **2007**, *43*, 229–240.
- (21) (a) Nagy, P.; Kettle, A. J.; Winterbourn, C. C. *Free Radic. Biol. Med.* **2010**, *49*, 792–799. (b) Nagy, P.; Kettle, A. J.; Winterbourn, C. C. *J. Biol. Chem.* **2009**, *284*, 14723–14733.
- (22) Spinks, J. W. T.; Woods, R. J. *Introduction to Radiation Chemistry*, 3rd ed.; Wiley: New York, 1990.
- (23) Bobrowski, K. *Nukleonika* **2005**, *50* (Supplement3), S67–S76.
- (24) (a) Buxton, G. V.; Stuart, C. R. *J. Chem. Soc. Faraday Trans.* **1995**, *91*, 279–281. (b) Schuler, R. H.; Patterson, L. K.; Janata, E. J. *Phys. Chem.* **1980**, *84*, 2088–2090.
- (25) Janata, E.; Schuler, R. H. *J. Phys. Chem.* **1982**, *86*, 2078–2084.
- (26) Buxton, G. V.; Greenstock, C. L.; Helman, W. P.; Ross, A. B. *J. Phys. Chem. Ref. Data* **1988**, *17*, 513–886.
- (27) Marciniak, B.; Bobrowski, K.; Hug, G. L. *J. Phys. Chem.* **1993**, *97*, 11937–11943.
- (28) Rusconi, F. *BMC Bioinform.* **2006**, *7*, 226.
- (29) (a) Rusconi, F.; Belghazi, M. *Bioinformatics* **2002**, *18*, 644. (b) Rusconi, F. *Bioinformatics* **2009**, *25*, 2741–2742.
- (30) Frisch, M. J.; Trucks, G. W.; Schlegel, H. B.; Scuseria, G. E.; Robb, M. A.; Cheeseman, J. R.; Scalmani, G.; Barone, V.; Mennucci,

B.; Petersson, G. A. et al. *Gaussian 09*, revision A.02; Gaussian Inc.: Wallingford, CT, 2009.

(31) Pettersen, E. F.; Goddard, T. D.; Huang, C. C.; Couch, G. S.; Greenblatt, D. M.; Meng, E. C.; Ferrin, T. E. *J. Comput. Chem.* **2004**, *25*, 1605–1612.

(32) (a) Chrysochoos, J. *Radiat. Res.* **1968**, *33*, 465–479. (b) Solar, S. *Radiat. Phys. Chem.* **1985**, *26*, 103–108. (c) Dizdaroglu, M.; Simic, M. G. *Radiat. Res.* **1980**, *93*, 437. (d) Lichtin, N. N.; Shafferman, A. *Radiat. Res.* **1974**, *60*, 432–440.

(33) Zegota, H.; Kolodziejczyk, K.; Król, M.; Król, B. *Radiat. Phys. Chem.* **2005**, *72*, 25–33.

(34) Malencik, D. A.; Anderson, S. R. *Amino Acids* **2003**, *25*, 233–247.

(35) Bansal, K. M.; Fessenden, R. W. *Radiat. Res.* **1976**, *67*, 1–8.

(36) (a) Hiller, K.-O.; Masloch, B.; Göbl, M.; Asmus, K.-D. *J. Am. Chem. Soc.* **1981**, *103*, 2734–2743. (b) Prütz, W. A.; Butler, J.; Land, E. J.; Swallow, A. J. *Int. J. Radiat. Biol.* **1989**, *55*, 539–556. (c) Prütz, W. A. In *Sulfur-centered reactive intermediates in chemistry and biology*; Chatgililoglu, C., Asmus, K.-D., Eds.; Plenum Press: New York, 1990; pp 389. (d) Prütz, W. A.; Butler, J.; Land, E. J. *Free Rad. Res. Comm.* **1986**, *2*, 69–75.

(37) (a) Hiller, K.-O.; Asmus, K.-D. *J. Phys. Chem.* **1983**, *87*, 3682–3688. (b) Asmus, K.-D. In *Sulfur-Centered Reactive Intermediates in Chemistry and Biology*; Chatgililoglu, C., Asmus, K.-D., Eds.; Plenum Press: New York, 1990; Vol. 197, pp 155–172. (c) Asmus, K.-D.; Göbl, M.; Hiller, K.-O.; Mahling, S.; Mönig, J. *J. Chem. Soc., Perkin Trans. 2* **1985**, 641–646. (d) Bobrowski, K.; Holcman, J. *Int. J. Radiat. Biol. Relat. Stud. Phys., Chem. Med.* **1987**, *52*, 139–144.

(38) Mozziconacci, O.; Bobrowski, K.; Ferreri, C.; Chatgililoglu, C. *Chem.—Eur. J.* **2007**, *13*, 2029–2033.

(39) (a) Vengadesan, K.; Gautham, N. *Biopolymers* **2004**, *74*, 476–494. (b) Ramya, L.; Gautham, N. *Biopolymers* **2012**, *97*, 165–176. (c) Zhan, L.; Chen, J. Z. Y.; Liu, W. K. *Biophys. J.* **2006**, *91*, 2399–2404. (d) Shen, M. L.; Freed, K. F. *Biophys. J.* **2002**, *82*, 1791–1808. (e) Hansman, U. H. E.; Okamoto, Y.; Onuchic, J. N. *Proteins: Struct., Funct., Genet.* **1999**, *34*, 472–483.

(40) Goshe, M. B.; Chen, Y. H.; Anderson, V. E. *Biochemistry* **2000**, *22*, 1761–1770.

(41) Solar, S.; Solar, W.; Getoff, N. *J. Phys. Chem.* **1984**, *88*, 2091–2095.

(42) von Sonntag, C. *The Chemical Basis of Radiation Biology*; Taylor and Francis: New York, 1987; pp 1–515.

(43) Prütz, W. A.; Butler, J.; Land, E. J. *Int. J. Radiat. Biol.* **1985**, *47*, 146–159.

(44) Schöneich, C.; Pogocki, D.; Hug, G. L.; Bobrowski, K. *J. Am. Chem. Soc.* **2003**, *125*, 13700–13713.

(45) Merenyi, G.; Lind, J.; Engman, L. *J. Phys. Chem.* **1996**, *100*, 8875–8881.

(46) Harriman, A. *J. Phys. Chem.* **1987**, *91*, 6102–6104.

(47) Wojcik, A.; Lukaszewicz, A.; Brede, O.; Marciniak, B. *J. Photochem. Photobiol. A: Chem.* **2008**, *198*, 111–118.

(48) Bobrowski, K.; Lubis, R. *Int. J. Radiat. Biol.* **1986**, *50*, 1039–1050.

(49) Mozziconacci, O. In *One-electron transfers in the enkephalins*; Université De Paris-Sud: Orsay, 2007.

(50) Bobrowski, K.; Schöneich, C.; Holcman, J.; Asmus, K.-D. *J. Chem. Soc., Perkin Trans. 2* **1991**, 353–362.

(51) Bergès, J.; Trouillas, P.; Houée-Levin, C. *J. Phys. Conf. Ser.* **2011**, *261*, 012003.

(52) Bobrowski, K.; Wierzchowski, K. L.; Holcman, J.; Ciurak, M. *Int. J. Radiat. Biol.* **1990**, *57*, 919–932.

(53) Kciuk, G. In *Influence of functional groups of aminoacids on the mechanisms of radical reactions in peptides containing tyrosine*; Institute of Nuclear Chemistry and Technology: Warsaw, 2011.

(54) Bobrowski, K.; Wierzchowski, K. L.; Holcman, J.; Ciurak, M. *Int. J. Radiat. Biol.* **1992**, *62*, 507–516.

(55) Ostuni, M. A.; Gelinotte, M.; Bizouarn, T.; Baciou, L.; Houée-Levin, C. *Free Radic. Biol. Med.* **2010**, *49*, 900–907.

(56) (a) Sicard-Roselli, C.; Lemaire, S.; Jacquot, J.-P.; Favaudon, V.; Marchand, C.; Houée-Levin, C. *Eur. J. Biochem.* **2004**, *271*, 3481–3487. (b) DalleDonne, I.; Milzani, A.; Colombo, R. *Biochemistry* **1999**, *38*, 12471–12480.